The Role of Wall Deposition and Re-Entrainment in Swirl Spray Dryers

Víctor Francia
School of Chemical Engineering, University of Birmingham, Birmingham, U.K.

Procter & Gamble R&D, Newcastle Innovation Centre, Newcastle upon Tyne, U.K.

Luis Martín and Andrew E. Bayly
Procter & Gamble R&D, Newcastle Innovation Centre, Newcastle upon Tyne, U.K.

Mark J. H. Simmons
School of Chemical Engineering, University of Birmingham, Birmingham, U.K.

DOI 10.1002/aic.14767
Published online March 29, 2015 in Wiley Online Library (wileyonlinelibrary.com)

A new experimental method is outlined to study fouling in spray dryers and similar devices. In essence, it makes the deposits traceable so that one can quantify the material that comes off the walls, how long it remains there and how the deposits agglomerate with particles in the air. This paper investigates a countercurrent swirl spray dryer of detergent and provides sound evidence that fouling is a dynamic process: clusters form and break at the walls renewing an active layer of deposits. Remarkably, the wall generates >20% of the product and most of the large granules, and increases drastically the residence time of the powder. The assumptions of current numerical models are clearly invalid (i.e. particles rebound at the wall or deposit indefinitely). Several re-entrainment mechanisms and their times scales are identified in this work, and accordingly, a new general framework to describe fouling in spray dryers is proposed.
AIChE J, 61: 1804–1821, 2015
Keywords: deposition, re-entrainment, fouling, resuspension, spray drying

Introduction

Fouling remains a fundamental issue in many industries. It involves the mechanisms by which discrete particles, clusters, floccules, or colloidal structures deposit at the walls of contained units and it is often a dynamic process, where the deposits are resuspended by the action of aerodynamic forces, gravity, or impacting particles. These phenomena constitute a formidable technical challenge in the petrochemical industry, engines, aerosol and medical applications, membranes and within many operations in the particle technology industry, from granulation to spray drying.

The underpinning physics of fouling is intimately related to the particle turbulence interaction.[1] As particle relaxation time increases, deposition and re-entrainment become governed by inertial effects and less influenced by turbulent flow. Several studies thus focus on the interactions between small particles and boundary layers, for example, on how coherent turbulent structures near the wall are responsible for unbalanced rates of deposition and ejection events.[2,3] These systems usually deal with single particles and monolayers, disregarding particle-particle forces and focusing on describing the interaction between the particles and the surface. Henry et al. review in detail the work in colloidal particulate fouling,[4] where a number of authors work in a multilayer description including the interaction force between the wall-borne clusters. A different approach to resuspension is based on the definition of a potential, or energy well,[5,6] which has been recently extended to a multilayer kinetic description.[7] Other important effects include the impact of swirling flows,[8] wall roughness,[9] or the formation of aggregates near the wall.[10]

The study of lower ranges of inertia focuses on short range adhesive and cohesive forces such as Van der Waals or electrostatics, and often associates the cause of re-entrainment to aerodynamic forces. However, gravity driven mechanisms such as the detachment of large sections, or shedding, are significant in other fields such as combustion, where ash deposition, aging, and shedding are widely recognized phenomena.[11–13]

The effect of particle impacts at higher particle inertia can also lead to resuspension. This has received little attention, not the least due to the difficulties in describing the microstructure at the wall.[14] Deposits in industry comprise of a wide range of different materials. This involves many

Additional Supporting Information may be found in the online version of this article.

Correspondence concerning this article should be addressed to V. Francia at v.francia.chemeng@gmail.com.

types of different interactions, cohesive forces, and aging processes. Reproducing their structure experimentally is extremely challenging, which explains the lack of data and the use of semiempirical models for design purposes.[15]

Regimes covering high particle inertias occur in the spray drying of products such as milk, instant coffee, pharmaceutical powders, ceramics, or detergents. Here, particles and droplets with a wide range of size, momentum, and composition coexist in the unit. The study of deposition and re-entrainment has mostly focused on cocurrent dryers and has been associated with three main issues: (1) product degradation and safety and quality concerns, (2) a detriment in the yield and the process efficiency, and (3) costs associated to maintenance.[16] The research in the context of the food industry reports ample evidence in this regard.[14] It provides the most relevant efforts in optimizing the yield[17–19] for which the role of resuspension[20] and new particle-wall contact models is emphasized.[21] Countercurrent spray dryers operate differently: they benefit from a strong turbulent swirling flow to increase particle residence time and obtain better energy efficiencies.[22] On the one hand, the counter flow causes an increase in particle concentration, promoting particle-particle contacts, and agglomeration[23] while on the other, the swirl generates a preferential concentration of particles near the wall, where certain size fractions tend to stagnation. This causes multiple wall impacts and much higher deposition rates. However, very few works pay attention to the wall processes in these units. In a detergent context, they were largely linked to operational issues[22] rather than to any significant effect to the process. The generation and breakage of particulate multilayers was acknowledged only recently by the visualization of the wall region in a restricted area[24] but a more detailed study remains a challenging task, because it deals with complex contact mechanics when deformable droplets or semidried particles impact a fixed substrate, comprised itself of clusters.

In cocurrent dryers, the yield decreases due to material accumulating at the wall.[16,20] However, it must be noted that swirl countercurrent towers operate for long periods of time without the need for cleaning. It follows that deposition is either suppressed, or balanced by the re-entrainment of material. Perhaps a more revealing question would be the time scale over which this equilibrium is reached. In general, the frequency of re-entrainment events in any given structure is owed to a balance between disruptive stresses and cohesive forces. If the stresses are low, large clusters are re-entrained, few events occur and their time scale is high, potentially larger than the process time scale. In this case, re-entrainment is observed as intermittent events and produces particles clearly identifiable by a large size and a different structure from the rest of the powder. This is for instance the case of shedding of ash deposits in burners.[12] On the contrary, if disruptive stresses are much higher than any bonds between particles or particles to the wall the re-entrainment events are much more frequent and particles spend no significant time in contact to the wall. The work presented in later sections confirms that the deposits seen in a swirl countercurrent detergent spray dryer are an intermediate scenario.[25] Disruptive stresses are comparable to the structural forces binding the clusters together and re-entrainment events become more frequent than in a shedding process. The time scale of the contact with the wall now approaches that of the process and the size of the resuspended clusters becomes comparable to the mean product size.[24] For that reason, the aggregates originated at the wall simply blend in with the rest of particles in the product, which explains why they have never been characterized.

Current numerical models of spray dryers assume that the wall has a minor contribution to the overall process and ignore any significant impact in particle residence time or growth, which have not yet been studied in detail. This is the purpose of this work. The following sections focus in the study of an industrial scale detergent countercurrent spray drying tower. They outline a tracer experiment that has permitted quantification of the re-entrainment, and analysis of its impact in the residence time of the solids and the size of the final product. The data underscore the errors associated with the omission of the wall processes in numerical models, failing to account major effects in the particle drying and growth of large part of the product, including the majority of granules of a size >850 μm.

Experimental Methodology

Unit design and operation

A spray drying tower, property of Procter & Gamble Co. was used in the experiments. The design and operation are depicted in Figure 1. The hot air is introduced at the bottom of the tower through a series of symmetrical air inlets denoted [5] in Figure 1, which impart downward and tangential components to the air velocity. Their action causes an air vortex to rise into the cylindrical section and the kinetic energy contained in the flow, in particular within the tangential motion, decreases due to the action of the wall shear stress.[26] On reaching the top end of the cylinder, the flow converges into the tubular guard or vortex finder, and exits toward cyclones [23] where the elutriated fines [26] are separated from the exhaust air [25].

A standard detergent formulation serves for the preparation of the slurry, which is comprised of aqueous, organic, and solid phases. It is generated in a batch mixer, known as the crutcher [7] by the addition among others of polymer(s), surfactant(s), and inorganic salt(s), for an overall content in solids between 30 and 60% in mass. A larger mixer, or homogenizer, known a drop tank [8] serves as the buffer for continuous operation. The slurry is then pumped at a low pressure into a hammer mill [13] to break agglomerates and avoid damage and blockages downstream. It is then brought to high pressure and conducted into the tower [15]. Atomization is performed from a single-swirl pressure nozzle that provides a hollow cone pattern.[22] It is located at the level $5.9D$ [17], at the centerline and aligned downward. Inspection areas at the walls are shown in Figure 2 and Table 1 summarizes the main operation conditions.

Three modifications were made to conduct the tracer experiments, see Figure 1: (1) an injection system for an aqueous solution of dye is installed at the low pressure line [11, 12], before the hammer mill; set to provide 100 ppm of a fluorescent dye, Sanolin Rhodamine B02, in the final particulate product; this dye is selected because it sustains the operating temperatures and provides a relatively high accuracy in visible spectrophotometry. (2) A set of water dual nozzles [21] is placed at the bottom of the dryer, feeding from a water storage tank at 60°C [20] and (3) a diversion of the slurry line [15] is installed before the nozzle arm [16], discharging into a storage tank open to the atmosphere [19].

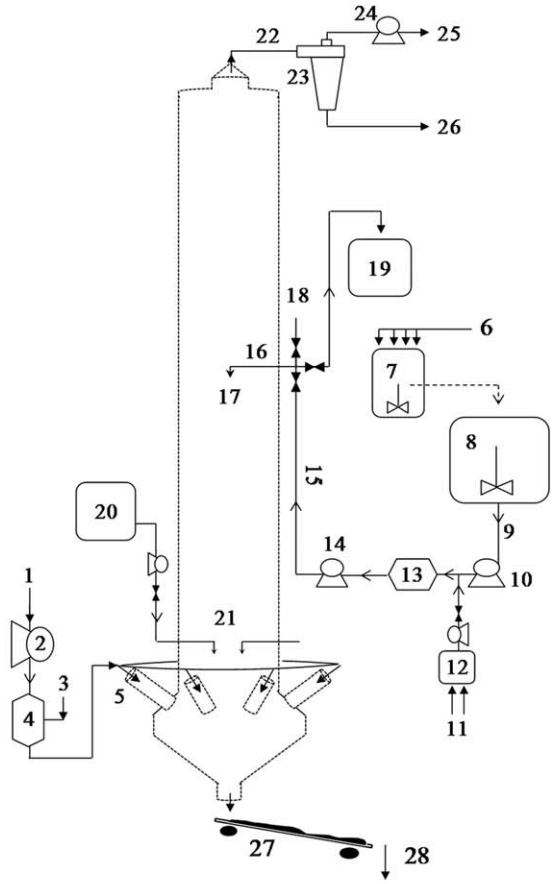

1- Ambient air feed
2- Hot air inlet air fan.
3- Fuel feed.
4- Burner.
5- Hot air inlet nozzle/s.
6- Slurry additions.
7- Crutcher. Batch low shear.
8- Drop tank. Continuous low shear.
9- Low pressure slurry line.
10- Low pressure pump.
11- Tracer and water feeds.
12- Storage. Tracer aqueous solution.
13- Hammer mill. Continuous high shear.
14- High pressure pump.
15- High pressure slurry line.
16- Nozzle arm.
17- Slurry pressure nozzle.
18- Purge. Air and vapour.
19- Slurry external storage.
20- Storage. Hot water.
21- Water dual nozzle/s.
22- Exhaust air line.
23- Cyclones.
24- Exhaust air fan.
25- Exhaust air oulet.
26- Exit product. Cyclones.
27- Tower belt.
28- Exit product. Tower belt.

Figure 1. A countercurrent swirl spray dryer.

The configuration of the lines of hot air, slurry and tracer injection.

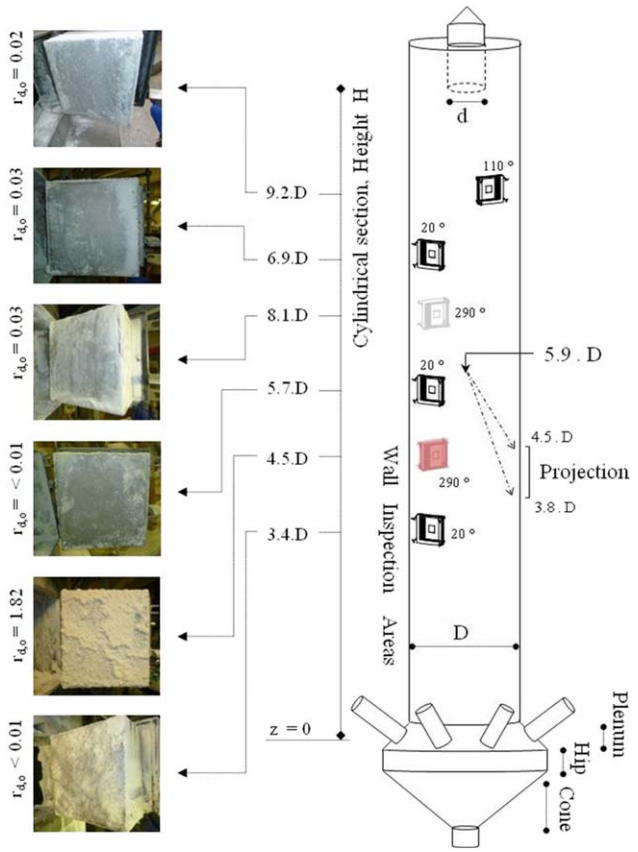

Figure 2. Location of nozzle, wall inspection areas, the projection of the spray cone (axi-symmetric) and the extractable plate at 4.5.*D*.

Wall deposits axial distribution in a replicate of the experiments described here, initial net deposition rate, $r_{d,o}$, given in g. s^{-1} .m^{-2}. [Color figure can be viewed in the online issue, which is available at wileyonline library.com.]

Sampling and measurement

Samples are taken at the exit of the tower belt [28] collecting the entire stream; they are sampled down and used for the analysis of particle size and the dye content. Size is analyzed by sieving using the Taylor series from 150 to 3350 μm, and the dye content is determined by the use of a UV/Visible spectrophotometer (Shimadzu UV-2401PC) at the maximum absorbance wavelength, 565 nm, with reference to a blank control solution. The morphology of each size class is analyzed using scanning electron microscopy (SEM; Hitachi TM1000) and the distribution of the tracer within the granule is studied under optical microscopy (Leica MZ16 A). The droplet size during atomization is obtained from laser diffraction measurements (Malvern Spraytec Particle Sizer, RTSizer 5.6) of sprays made using an external rig that replicates the operation of the industrial scale unit. The droplet size distribution and the spray angle associated to the operating conditions given in Table 1 are measured from several spray durations between 1 and 2 s.

The walls are monitored at the inspection doors depicted in Figure 2. During steady-state operation, the net initial deposition rate is measured at six different wall inspection surfaces. The amount of material deposited during 10–15 min is taken, starting with a clean surface each time. Not all locations show similar rates, or the same type of deposits in Figure 2. The material deposited above the nozzle contains high moisture levels but the initial net deposition rate, $r_{d,o}$, is small and deposits are thin. Moving down, the deposits become drier and more brittle, until the bottom end where no significant deposition occurs. The sections nearby the nozzle show the highest levels of deposition. These are the areas where the hollow spray cone projects onto the wall (see the projection area according to the spray angle in Figure 2). Here, multiple droplets with high inertia impact the deposits, generate the outer layers, and cause large pieces to detach, flowing downward close to the wall.[24] This particular location is monitored separately, see level 4.5 *D* in Figure 2. A dismountable plate has been designed to be flush with the

Table 1. Design Features and Operating Conditions for the Stages Defined in Figure 4

Tower Design Parameters								
d/D	0.29	H/D	10.58	[a]Ω_i	5.1–5.4	[b]$U_{p,sd}$	<2 – 3 m/s	[b]$U_{p,w}$	<10 m/s
Stage		P−1	CH−1		P−2		CH−2		P−3
S, Slurry line; W, Water lines; P, Product in the tower belt; E, elutriated fines; EP, full exiting power[c]									
$\bar{M}_s/\bar{M}_{s,\mathrm{P-1}}$		1.00 ± 0.02	0		1.00 ± 0.03		0		1.01 ± 0.03
$\bar{M}_w$ /$\Delta\bar{M}_{\mathrm{Eq}}$		0	0.88		0		0.88		0
$\bar{M}_E$ (% $\bar{M}_{\mathrm{PE}}$)		2.8	–		n/a		–		n/a
$\bar{T}_P - \bar{T}_S$(°C)		-3.5 ± 3.6	–		-2.5 ± 3.9		–		-5.3 ± 4.0
A, Air; IN, inlet; EX, exhaust conditions; cone, at the cone.									
$\bar{M}_A/\bar{M}_{A,\ \mathrm{P-1}}$		1.00 ± 0.02	0		0.97 ± 0.03		0		0.97 ± 0.02
$\bar{T}_{A,\mathrm{IN}}$ (°C)		264.9 ± 2.6	264.4 ± 1.5		264.4 ± 2.7		267.5 ± 4.0		264.4 ± 4.3
$\bar{T}_{A,\mathrm{EX}}$ (°C)		88.3 ± 0.5	108.2 ± 8.1		89.6 ± 0.4		107.2 ± 7.6		91.2 ± 1.9
$\bar{T}_{A,\mathrm{cone}}$ (°C)		195–206	191–199		195–198		176–186		194–198
rH_{EX} (%)		15	6		14		7		14

[a]The initial swirl intensity, Ω_i, or swirl number, is defined as the ratio of angular momentum of the inlet flow to the momentum in the cylinder based on the superficial velocity times the cylinder radius.[26]
[b]Particle sedimentation velocity $U_{\mathrm{p,sd}}$ ranges from negative values to up to 2–3 m/s. depending on size. Numerical simulations of the spray estimate wall impact velocities $U_{\mathrm{p},w}$ to be <10 m/s. for sizes <400 μm. Impacts thereafter occur < 1–2 m/s.
[c]M, mass rate; rH, relative humidity; $\Delta\bar{M}_{\mathrm{Eq}}$, equivalent rate of water contained in the slurry.

inner wall of the cylinder, such that a section of the wall can be, in effect, extracted, weighted, and placed back in position at different times.

The Renewal of Particulate Multilayers

Description of air-borne and wall-borne states

The deposits may be regarded as a continuous structure that is different from the particles flowing in the air. The material within the exit powder can, therefore, possess a wall or air-borne origin according to whether it has been at any point part of the structure fixed at the wall. On these bases, the dryer may be defined by the two different regions depicted in Figure 3a: (1) the air-borne region comprised by the air vortex that contains a population of air-borne particles, and (2) the wall-borne region comprised by the deposits that remains fixed. Both are described in Figure 3b as spatially distributed reactors where the solids undergo different transformations. In the air-borne reactor, they dry, aggregate, and flow, and in the wall-borne reactor, particles dry and may sinter but remain fixed. Both regions interact by a mass flow rate of particles that move from an air to wall-borne state and vice versa by deposition, r_{d}, and re-entrainment, r_{e}. In reality, these rates are distributed through the height of the tower and vary according to the local drying conditions, the deposit properties and the local rate of impacts onto the wall.

Outline of the tracer experiments

Decoupling experimentally, the wall and air-borne processes requires determining the exchange rate between both reactors in Figure 3b and the particle residence time in each. This work studies only the wall-borne reactor, for which it is important to quantify the average rate of re-entrainment r_{e} and the time the particles spend resident in the deposits. These data have been generated by tracking the release of the material contained in the wall-borne reactor during a full renewal cycle, in the same way "wash-out" tracer experiments do in chemical reactors.[27] In the real dryer, the requirement is to ensure at a given point in time that the material borne at the wall contains a known tracer concentration while that in air-borne state contains none. Several stages will be followed to achieve this. Initially, the unit will be brought to a standard production rate to generate a stable layer of deposits, at this point untraceable. Then, the dye solution will be injected such that atomized droplets have certain dye content and deposition and re-entrainment at the wall produces layers of traceable material. The unit will then be emptied of air-borne particles leaving behind a set of traceable deposits. At this point, atomization will be restarted with all droplets containing no tracer. The rate of release of the dyed material from the walls is then quantified by measuring the amount of tracer exiting in the product. In this way, the origin of aggregates can be determined, differentiating those that are generated from re-entrainment of material at the wall (dyed) from those with a pure air-borne history (white).

This experimental sequence is illustrated in Figure 4 and detailed below. The steps are designed to preserve at all times the operating conditions in the tower and maintain the properties of the deposits.

Generation and tracking of a set of active wall deposits. Sequence of a "wash-out" experiment

1. P−0. *Start up:* The rates of slurry and hot air ramp up to heat the unit and develop an initial layer of deposits associated with the particle-wall contacts.
2. P−1. *Production:* Production is carried out in a steady state. The product is characterized and the multilayer structure of deposits is formed at the walls.
3. CH−1. *Changeover. Connection of the dye injection:* Homogeneous mixing of the slurry and the dye is ensured by placing the injection before the hammer mill in Figure 1. However, the long residence time between

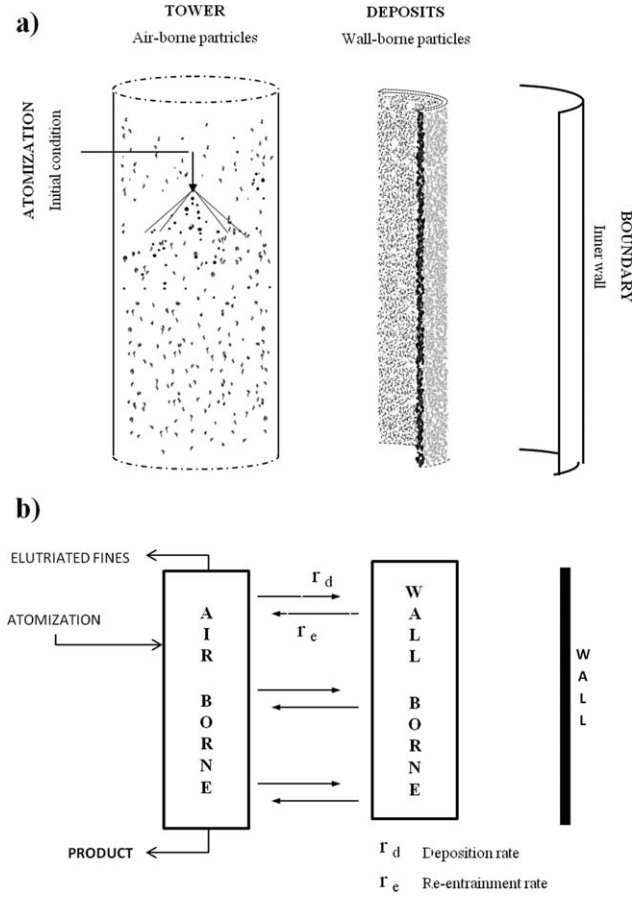

Figure 3. Description of particle history as a combination of two parallel reactors associated to the air and wall borne states.

the injection point and the nozzle (from stage [12] to [17] in Figure 1) causes a certain axial mixing of the tracer in the slurry line. Two requirements need careful consideration, (1) deposits tractability: a sharp step change in dye content at the nozzle is necessary to ensure only droplets of known concentration, either the target or zero are produced, and (2) deposits mechanical properties: the mechanics of deposition and erosion is the aim of the experiment, and thus the properties of the deposits should be maintained. According to these two objectives, the following sequence is executed. The dye injection starts and the next two changes are done simultaneously:

- The slurry line is diverted to an external loop connected to the atmosphere, where it discharges into a container for visual inspection, denoted [19] in Figure 1. After this, the nozzle arm itself is purged in [18] with water vapor to avoid solidification and the blockage of the line.
- Hot water is diverted into a pair of dual nozzles in [21]. Both spray a fine water mist into the conical region, with a combined rate set to match the evaporation rate when the slurry nozzle is in operation.

In operation, most of drying occurs at the bottom of the chamber. As the evaporation rate is kept constant with the use of the water nozzles, the air operating conditions can be left unchanged and in this way, the deposits in the cylinder are subject to similar air temperature, humidity, and velocity at all times. Nonetheless, in certain areas the deposits are likely not in equilibrium, but slowly drying so to minimize any change in their properties, the length of CH−1 was reduced as much as possible. Visual inspection and analytical measurements from [19] confirm the point when the tracer achieves a target constant concentration in the slurry. At this point, the line is ready to be diverted back into the tower.

4. P−2. *Production. Generation of traceable deposits*: The water flow is stopped in [21] and simultaneously, the slurry containing the target tracer concentration is diverted back from the external loop in [19] to the atomizer in [17]. All settings, including the burner, mixers, pumps, and temperature control remain unchanged, and thus the atomization pressure and subsequently the droplet size, returns almost instantaneously to the steady-state values of P−1. Production resumes and the exit powder in [28] and [26] starts showing the color derived from the dye. This continues for 3900 s, what will be proven sufficient to ensure that active layers in the deposits have been renewed and are now comprised of the traceable material. In the last 300 s, product is sampled for characterization.
5. CH−2. *Changeover. Disconnection of the dye injection:* At this point the air-borne and wall-borne reactors in Figure 3b are both full of dyed particles. To track the material exiting the wall-borne reactor one needs first, to empty the air-borne reactor and then, ensuring that the new population of incoming droplets contains no dye. To do this, the same changeover is executed, but in this case proceeding to the disconnection of the dye. The slurry is diverted out of the tower into external container [19] and instead the water is connected. The slurry loses the color and analytical measurements from [19] confirm the point when the dye concentration is $<1\%$ of the target.
6. P−3. *Production. Renewal of the wall deposits:* At this point, the reverse changes are made. The water flow is stopped and simultaneously the slurry which now contains no dye is diverted back to the nozzle in [17]. At this precise point in time, the tower is empty, the entire mass of deposits contains a given concentration of tracer and the entire population of air-borne droplets contains none. This situation is equivalent to setting a target tracer concentration in the material within the wall-borne reactor in Figure 3b, while the air-borne reactor is empty. When atomization restarts, the tower fills up, and samples are taken in [28] for a period of 3300 s, in such a way that the presence of the dye reveals the contribution of the resuspended material to the product.

A note in the solid hold up and the correct conditioning of the deposits during changeovers

The potential disruption of the deposits during the changeovers could be recognized by three signals: (1) visible changes in their morphology, (2) product exiting the tower belt or the cyclones, or (3) stagnation of solids hold up in the air. The inspection of the wall deposits is discussed later and shows no significant changes during the changeovers. In addition, no powder was seen to exit the unit in these periods. No powder exited from the tower belt, which indicates that detachment of large pieces due to gravity is not significant and at the cyclone exit, a negligible flow was observed.

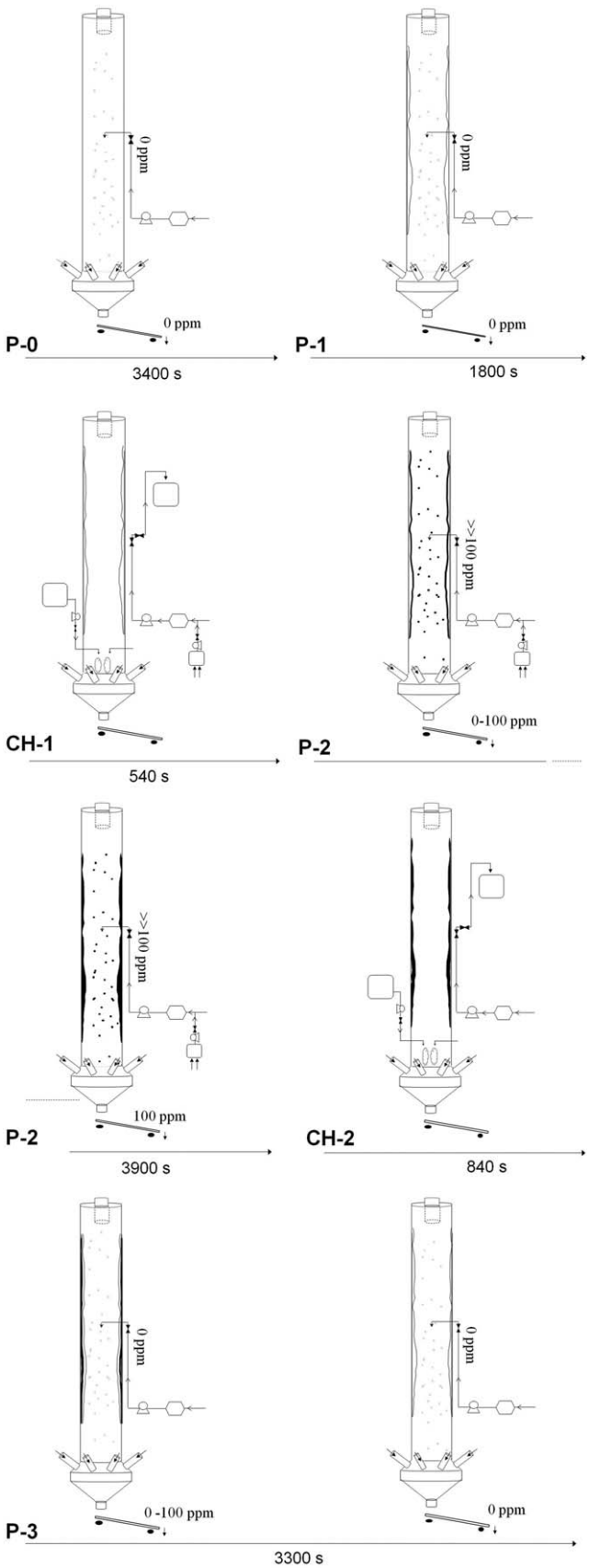

Figure 4. Stages of a tracer experiment sequence.

At the end of CH−1, the tower is assumed to be empty, but it might have contained solids stagnated due the counter flow. Evaluation of this is essential to keep the tractability of the deposits (i.e. ensuring that when the atomization restarts in P−3 the only particles in the unit that contain the dye are borne at the wall). This has been confirmed in a separate experiment. The same sequence was repeated but in this case, at the end of CH−1 the water nozzles and the air system were both shut down simultaneously. The solids hold up exited through the tower belt and were collected. The amount represents <0.4% of the weight of the deposits and a negligible concentration in the dryer. It is noticeable that after 25 min of the shutdown, a larger section of the deposits detached (4.5% of the full weight). This highlights the impact that the air conditions have in the deposits properties, and the success of this sequence in preserving them.

Results and Discussion

Transient production

When the unit fills up in P−3, the mass rate of powder exiting from the bottom, denoted M_P, increases before reaching its steady-state value, $M_{P,St}$. This evolution was determined in a separate experiment. The same sequence was replicated and when the atomization restarted in P−3, M_P was measured manually. Figure 5a presents the evolution of both the rate and the product size distribution during P−3. It is clear from both that it takes ~100 s for the unit to fill and achieve the steady-state concentration. This is in agreement with the particle air-borne residence times <30–45 s reported for similar units[22,28] and more recently for the same spray dryer.[29,30] The initial size distribution is very narrow and contains primarily the size fractions that later become the mean product size between 300 and 600 μm. As time progresses, the distribution spans to contain a larger proportion of small and large sizes. It is stabilized close to the average size distribution at steady state for times $t > 100$ s. It is a noticeable fact that both larger and smaller size fractions take longer to exit, as one expects the sedimentation of large granules to be much faster. This could be explained by the fill up, if large aggregates are formed only when particle concentration rises sufficiently. However, it is most likely related to a high level of interaction with the walls, discussed in detail later.

Steady-state production

Figure 5b compares the size distribution of the droplets and the product across the entire experiment in stages P−1, P−2, and P−3. The atomization covers a range from 20 to 1000 μm and is skewed over the large sizes, having a mode from 350 to 450 μm, a median volume size of $x_{p,50}=292$ μm, and 10th and 90th percentiles, $x_{p,10}$ and $x_{p,90}$, of 85 μm and 530 μm respectively. The product undergoes a significant particle growth, the distributions covering a range from 70 to 10000 μm. They all present a mode between 300 and 400 μm, a median mass size $x_{p,50}$ ranging from 360 to 430 μm and $x_{p,10}$ from 160 to 180 μm. From the early stages in P−1, the size distribution in Figure 5b shows a long tail >1000 μm. However, as the time progresses it becomes larger and $x_{p,90}$ increases from 1350 μm in P−1 to significant higher values, 3234 and 2450 μm in P−2 and P−3. Stable operating conditions are reached in all cases, including relatively constant heat losses in the dryer. However, the product

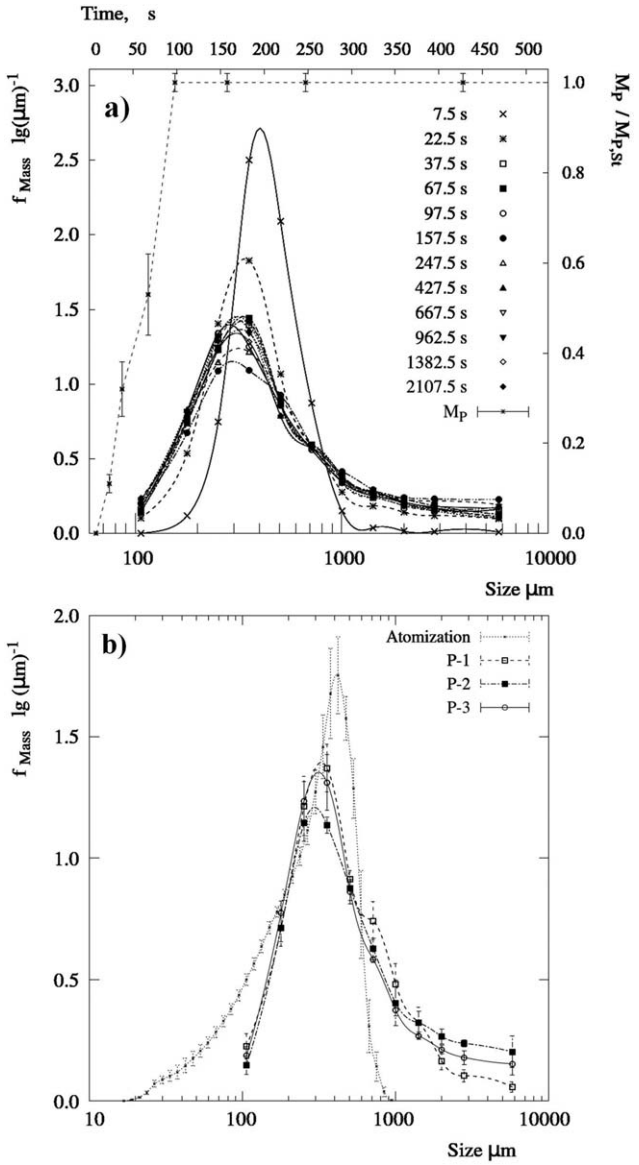

Figure 5. (a) Evolution of the product exit rate (right and top axes) and size probability density function (left and bottom axes) during P−3. (b) Comparison of the size probability density functions of the droplets and the product during P−1, the final stage of P−2, and P−3.

size evolves during a period of >7200 s, which is much higher than the residence times involved in particle flow. This indicates that during the initial stage in P−1, processes other that fluid dynamics must still be in a transient state. The next section associates this effect with the stabilization of deposition and re-entrainment rates.

Deposition and re-entrainment equilibrium

Figure 6 presents photographs of the extractable plate located at the wall in the level 4.5 D taken during the entire experiment. In parallel, Figure 7 provides the evolution of the weight of the ensemble (plate plus deposits) associated to the same images. In the start-up, P−0, deposition increases until the product covers the entire surface. During this period, the weight of the deposits rises linearly in Figure 7, at a constant net deposition rate, $r_{d,o}=1.83$ g s^{-1} m^{-2}. After this stage, the weight on the plate stabilizes. No significant variations can be related to either of the changeovers, which indicate that the mechanical properties of the deposits have been kept within reasonable margins. The tendency to achieve a maximum weight or thickness, where the net deposition rate falls close to zero, is a common observation in particulate fouling, known as the "blocking effect."[4] In cases of low inertia and cohesive forces, it is in part related to re-entrainment and in part to the suppression of deposition.

A similar evolution was reported in swirl spray dryers[24] at higher cohesive forces and particle inertias, but until now its root cause remained unclear. Figure 6 shows that when the spray varies from white to dyed to white again, from P−1, P−2, and P−3, a change follows in the color of the deposits. This confirms there is deposition of atomized droplets (i.e. a similar color change in the deposits is also observed at all other locations with significant deposition in Figure 2). But further on, as the color change occurs, the weight of the ensemble given in Figure 7 remains constant. This is a major and important result: it provides the first experimental evidence of significant wall dynamics in these units. It demonstrates that the rates of deposition r_d and re-entrainment, r_e are in equilibrium in this section, and that such a renewal process is responsible for suppressing the growth of the deposits. Notice that they change sharply in color, not gradually and thus the structure must be renewed quickly. New sets of clusters must be brought from the air into the structure to be re-entrained back into an air-borne state a given time later.

Quantification of the re-entrainment rate

The detergent slurry contains three different phases, and it is noted that the dye used in this work distributes preferentially within the organic phase and therefore, dye and surfactant contents are correlated. The surfactant(s) level in the product varies across different sized particles,[31] primarily for the sizes <212 μm, and accordingly, pure dyed particles present a similar variation. For this reason, the reference dye content was obtained for each size class using the pure dyed powder obtained at the end of P−2. X is defined in Eq. 1 as the ratio between the dye content of a mixture and that of the pure dyed powder of the same size ranges, for a given sampling time t

$$X_{s,t}=\frac{S_{s,t}\cdot A_{s,t}}{S_{s,\mathrm{ref}}\cdot A_{s,\mathrm{ref}}} \tag{1}$$

X is equivalent to the ratio of dyed material present in the mixture. Notice that during P−3, the dyed material has a single possible origin: the deposits, and therefore, X is equivalent to the ratio of material that in fact, has a wall-borne origin, that is, the material that was part of the deposits and was resuspended after the atomization starts in P−3. The use of Eq. 1 carries a certain error when the deposits have a different content in surfactant(s) or tracer than the product. All the data reported here include a largely conservative estimate of this uncertainty.

Figure 8 presents the evolution of X for all size fractions in the samples taken during P−3. When atomization starts, the entire mass of deposits is dyed and the entire population of air-borne droplets is white. Droplets and particles start falling down and impact to the wall causing either deposition or re-entrainment. The first set of dyed re-entrained clusters

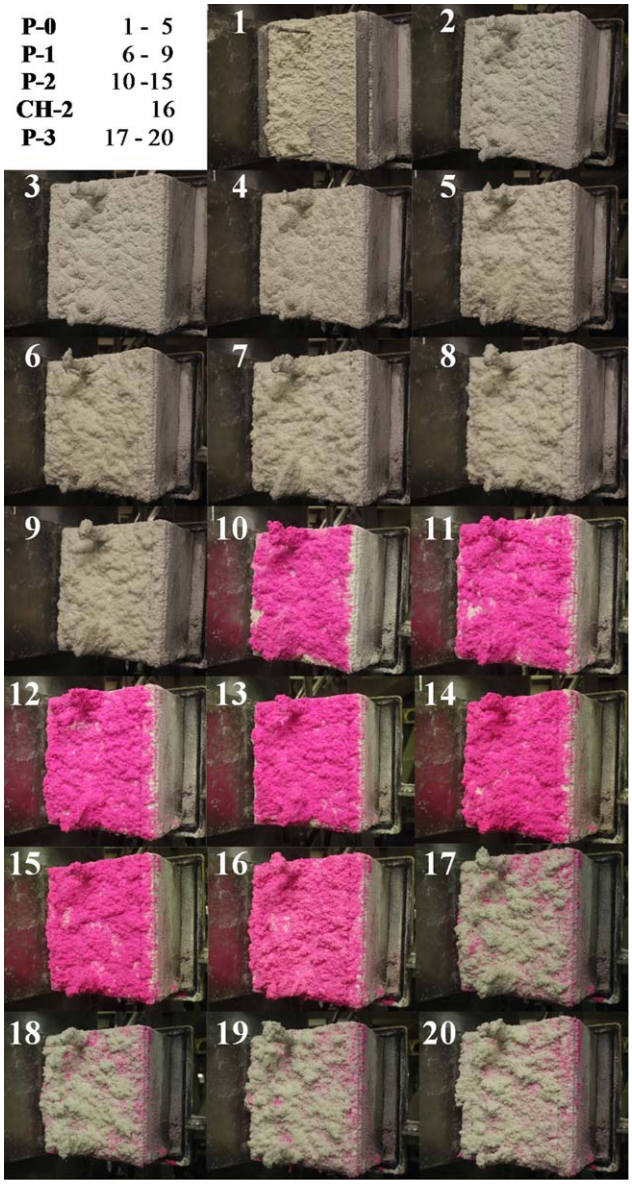

Figure 6. Evolution of the deposits observed at the inspection level 4.5.*D* containing the extractable wall plate.

[Color figure can be viewed in the online issue, which is available at wileyonlinelibrary.com.]

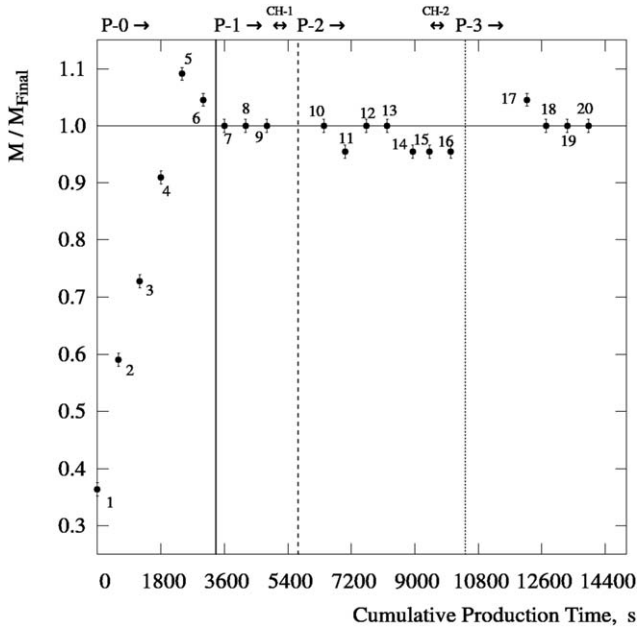

Figure 7. Evolution of the weight of the extractable wall section (plate plus deposit) shown in Figure 6.

joins then rest of air-borne powder and is delayed a given time before exiting due to the flight between the re-entrainment position and the exit. Thus, when the product begins to exit the tower (i.e. $t=0$ s) the exit rate of dyed material X corresponds exactly to the re-entrainment rate r_e. In this system, sampling is required and thus it is not possible to provide an instantaneous measurement of X at $t=0$ s. However, r_e is quantified by the value of X at the first sample, X_o, shown in Table 2, which can be considered an underestimation (across the initial sampling time $\sim$15 s). As time t progresses, the deposits and the re-entrained granules start containing white material, which makes X to diminish. Averaged values are computed for the full product and different size ranges using the data in Figures 5a and 8. During the fill up period ($\sim$100 s), the overall average value of X decreases from the initial sample $r_e \sim X_o = 20 \pm 1$ % of the production rate to 12 ± 1%. This range increases to values between $X_{o,<212\,\mu m} = 31 \pm 1$ % and 15 ± 1 % for the powder <212 μm, and up to values between $X_{o,>850\mu m} = 37 \pm 3$ % and 10 ± 1 % for the powder >850 μm.

These observations have major implications to the general view of the behavior of swirl countercurrent spray dryers. In a detergent context, a significant fraction of the product, at least 12% and most likely >20%, is not material originated at the nozzle but is material generated from the wall deposits and its size, structure, and drying history is related to the physics governing fouling (i.e. deposition, aging, and erosion of a network of clusters). These values become even more relevant for smaller and larger aggregates, known to have

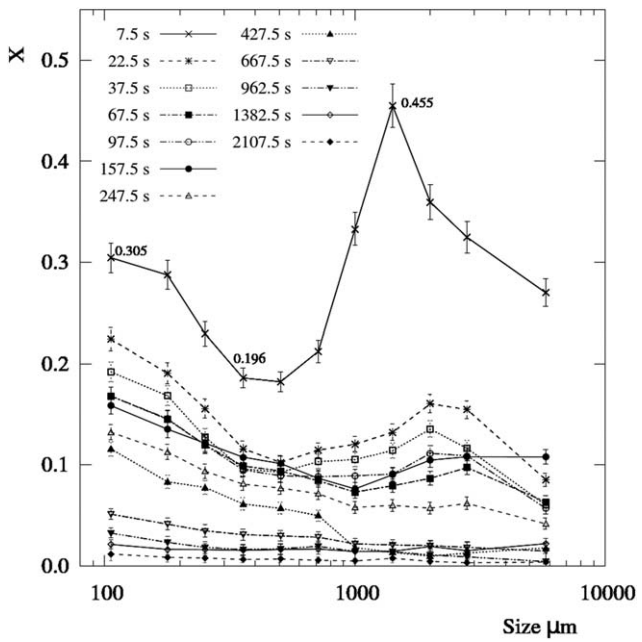

Figure 8. Ratio of dyed material of a wall-borne origin, *X*, in the samples taken during P−3.

higher water contents and a significant impact in the energy balance.[31] Furthermore, notice that this article only tracks the material that has become fixed at the walls. Any clusters forming and breaking at the wall but not becoming permanently fixed, or deposition and re-entrainment cycles that occur much faster than the first sampling time ~15 s blend in with the air-borne material, appearing as white material in the product. On this basis, the ranges given for X_0 are minimum estimates of the removal where the fastest interactions with the wall are not included, and thus the interaction with the wall can be higher.

Granule structure and morphology

Figure 9 provides some examples of the morphology observed under SEM analysis, and Figures 10 and 11 illustrate the analysis of the exit powder under optical microscopy. Figure 10 shows micrographs of the product exiting at the average mode age determined later as $t \sim 157.5$ s and at the initial sample $t \sim 7.5$ s, and Figures 10b and 11 provide details on the structure of the mixtures between air-borne droplets and wall-borne clusters. A collection of micrographs is also available in Supporting Information.

Small and Average Size Particles <850μm. Lower size fractions shown in Figure 10a are comprised, in general terms, of pure particles, either completely white or dyed. Several observations follow. First, the history of pure dyed particles must involve no aggregation with any air-borne droplet. This includes (1) the time they had remained wall-borne, potentially sintering with newly deposited droplets or subject to impacts, (2) the contact with other particles during the re-entrainment mechanics itself, and (3) the air-borne history from re-entrainment to exit. Second, despite the fact that no aggregation occurs, the detachment has been triggered by the impacts of air-borne particles. No particles exit during the changeovers nor are they hold up in the air when tower is empty and the deposits are subject to the same stresses due to gravity or aerodynamics.

The re-entrainment of pure dyed particles must follow two potential mechanisms, discussed in more detail in the last section of the article. First, the impacts of dry particles causing a direct detachment: in this case, both, particles and deposits are dry enough not to develop sufficient adhesive forces and cause deposition or capture, but the impacts contain a large enough inertia to break the bonds between the clusters. Second, the detachment of large pieces: being typically of a low density and heterogeneous shape, large clusters are unlikely to retain their shape and break down into smaller particles.[24] The detachment of large pieces can be triggered by the action of gravity alone or combined with the impact of dry particles or wet droplets. Note that the breakage of individual bonds in the multilayer structure can, in combination with gravity, lead to detachment of a large section.

Large Particles >850μm. The morphology of the large granules is itself heterogeneous (see Figure 9 and Supporting Information). In general, they present a variety of nonspherical structures and a high aspect ratio. Primary particles appear to be fused together forming granules with wide cavities, comparable in size to the primary particles that they contain. When particles collide between each other or to the wall, such surface features surely lead to a very different behavior from spheres, especially with regard to interlocking and rotation. Figure 9 includes several examples showing a

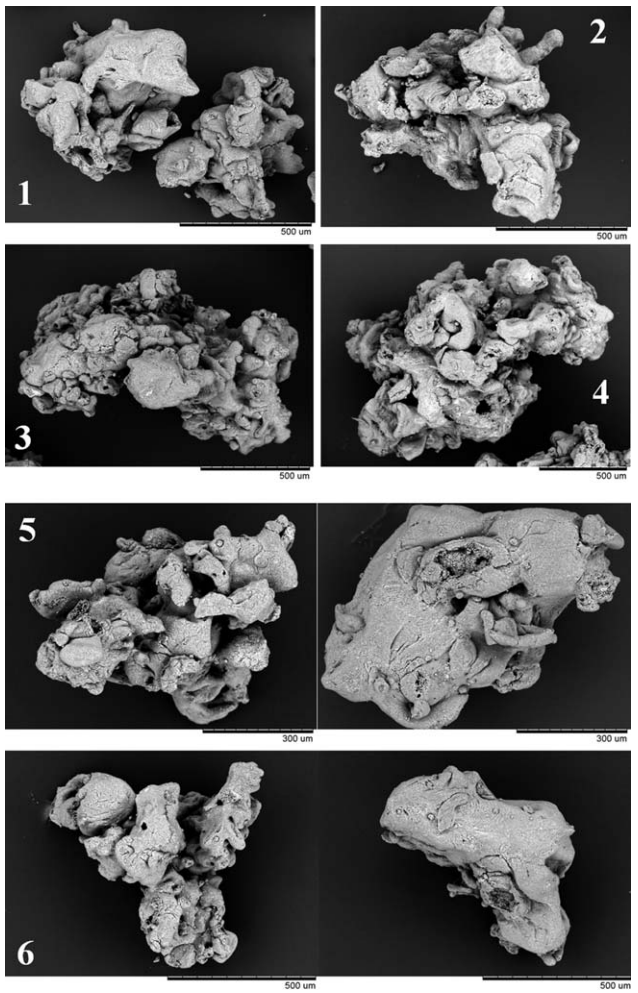

Figure 9. Structure of large granules under SEM.

Micrograph (1) correspond to the size fraction 450 μm < x_p < 600 μm; (2) to 600 μm < x_p < 850 μm; (3) to 850 μm < x_p < 1180 μm; and (4) to 1180 μm < x_p < 1800 μm. Micrographs (5, 6) show both sides, front and back, of the same granule for the size fraction 450 μm < x_p < 600 μm.

clear heterogeneity in particles having smooth and aggregated sides. This feature could be explained by the interaction with the wall. In a two-dimensional multilayer, sides can be exposed or not to sintering, and subject or covered from air-borne collisions.

In large granules, the wall-borne, or dyed, material is distributed in a different manner. In part, they are also comprised of identifiable pure dyed particles, which indicate the presence of a similar production mechanism as for the smaller particles. However, the remaining aggregates are not purely white but, as illustrated in Figures 10b and 11 they are in general mixtures of air-borne and wall-borne material. Figures 10b and 11-1 to 11-5 provide examples of the external distribution of dye. Aggregates range from pure dyed particles, to white granules with colored sections (e.g. Figures 10-7 to 10-9, 11-1, 11-2) and embedded dyed primary particles (e.g. Figures 10b-13 to 10b-15 and 11-3 to 11-5), and to other mixtures where the graduation in the color intensity at the surface results from an outer layer of white material, varying in thickness (e.g. Figures 10b-10 to 10b-13). As the time progresses, the deposits turn white and mixed granules containing only small sections of

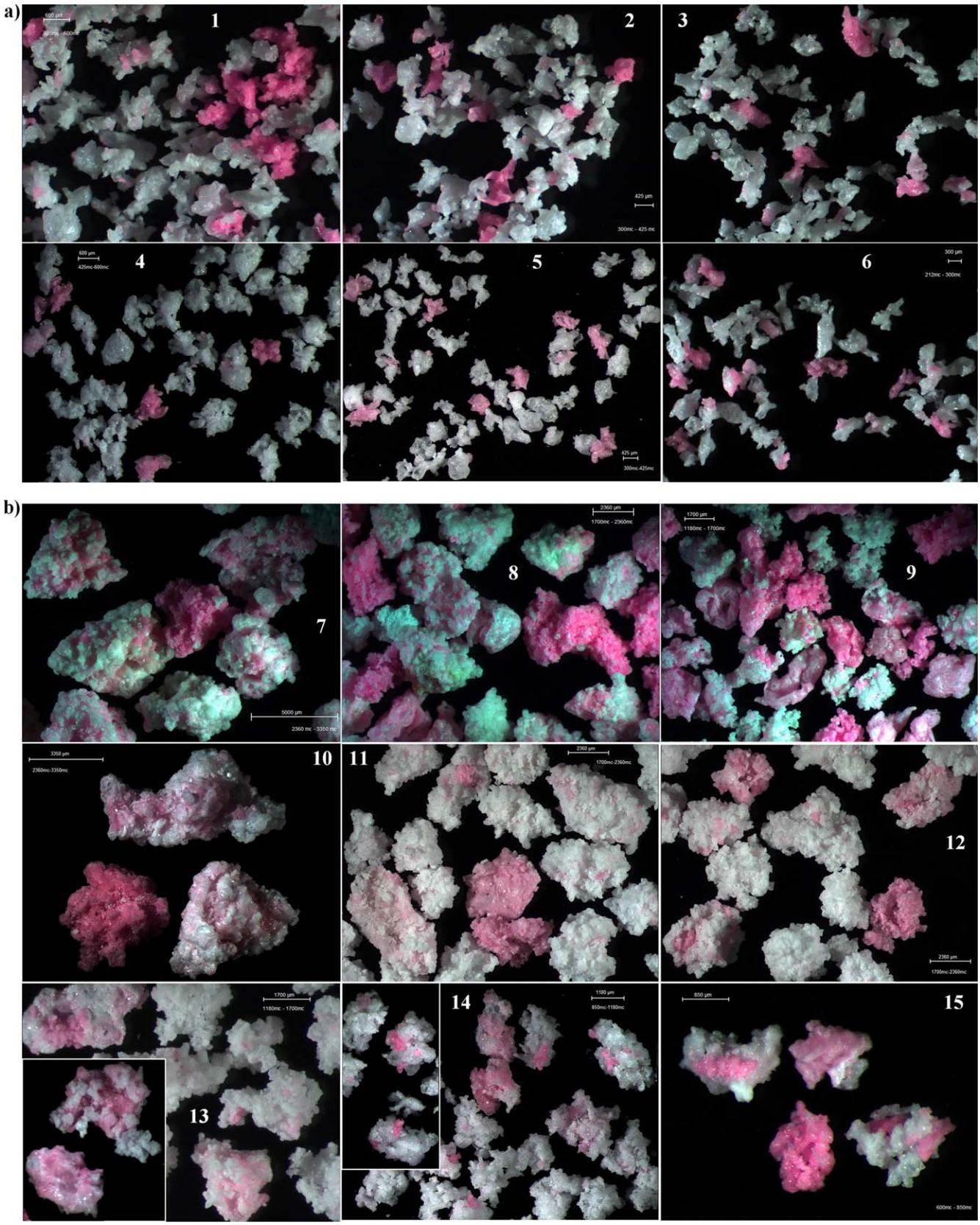

Figure 10. Dye distribution.

(a) Pure particles for x_p<850 μm, (b) mixtures particles for x_p>850 μm. For the initial sample ~7.5 s in (1 to 3, 7 to 9) and the mode ~157.5 s in (4 to 6, 10 to 15). Micrographs (1, 4) show the size fraction 425 μm<x_p<600 μm; (2, 5) to 300 μm<x_p<425 μm; (3, 6) to 212 μm<x_p<300 μm; (7, 10) to 2360 μm<x_p<3350 μm; (8, 11, 12) to 1700 μm< x_p<2360 μm; (9, 13) to 1180 μm< x_p<1700 μm; (14) to 850 μm< x_p<1180 μm and (15) to 600 μm<x_p<850 μm. Scale bars denote the upper limit the size fraction. [Color figure can be viewed in the online issue, which is available at wileyonlinelibrary.com.]

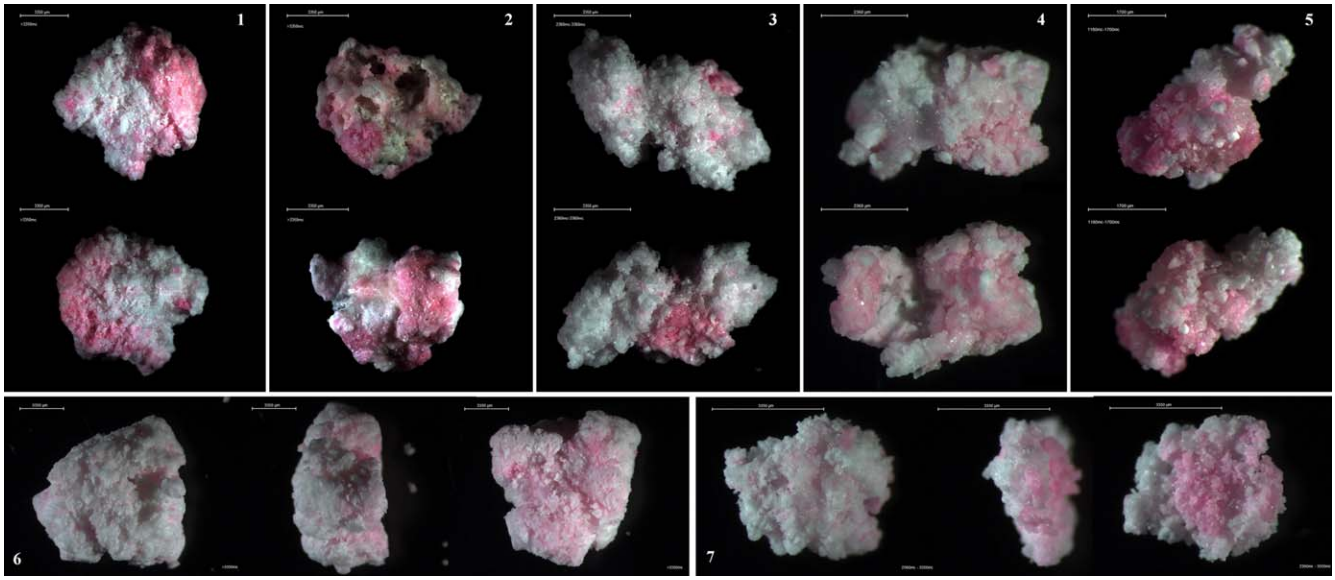

Figure 11. Mixtures in large granules.

External distribution of dye (1 to 5) presenting both sides (front and back) of the same granule. Internal distribution of dye (6, 7) presenting cut down granules, from left to right, the outer surface, the cut side, and the inner section. Micrographs (1, 2, 6) show the size fraction x_p>3350 μm; (3, 7) to 2360 μm<x_p<3350 μm; (4) to 1700 μm<x_p<2360 μm; (5) to 1180 μm<x_p<1700 μm. All scale bars denote to the upper limit of the size fraction. [Color figure can be viewed in the online issue, which is available at wileyonlinelibrary.com.]

colored material become common. However, after the tower has been filled (i.e. ~ 100 s) the largest fractions still contain $>10\%$ of dyed material, which indicates the dye is present in the inner structure of the granule. The internal distribution of the dye varies from homogeneous mixtures containing multitudes of white and dyed primary particles to granules where a dyed wall-borne nucleus has been captured by white air-borne material (e.g. Figures 11-6, 11-7). Further details are available in Supporting Information.

This analysis demonstrates that wall-borne clusters undergo aggregation with atomized material. This is a revealing fact. It indicates that the production of most large aggregates in the product is driven by the dynamics established at the wall. In this sense, the re-entrainment rates given earlier should be taken as an indication of the mass that is re-entrained from the deposits and exits within large individual granules, but noticing that in fact, most if not all of these particles are affected by the cycle of deposition and re-entrainment. Aggregation might occur at the wall, or close to it after the material has been re-entrained. However, it is worth noticing that the recirculation of solids from the wall into the proximities of the nozzle is very unlikely. Due to the swirl particles migrate outward; most of them flow down close to the wall and the smallest particles are recirculated up, but turbulence is no sufficiently strong to disperse them inward, what occurs only near the top end. This, in addition to the lack of mixtures observed <850 μm suggests that the recirculation of powder is not the cause of the generation of the mixtures. The last section of this article discusses other aggregation mechanisms linked to the re-entrainment.

In conclusion, the manner in which the wall-borne material distributes in the exit granules is correlated with their size. Small and average sizes are in general terms re-entrained as pure aggregates. Large size classes can also be re-entrained directly but in the majority of cases the process involves the aggregation between wall clusters and air-borne droplets.

Residence time of the re-entrained material

The age distribution, AD, of the re-entrained material can be quantified by measuring the exit rate of dyed material in P−3 at the intervals defined by the sampling times, similarly to a "wash-out" type of experiment.[25,27] Samples cover the full renewal cycle of the deposits in 3300 s. The average exit rate of wall-borne material is denoted w and given in Eq. 2 for the size class s and time interval i between the i^{th} and $i^{\text{th}-1}$ samples. It is function of the exit mass rate, M_P, and the ratio of material of wall-borne origin, X, given in Figures 5a and 8. A standard age probability density function, E, is estimated in Eq. 3 normalizing w by the total re-entrained mass, W. The latter is obtained in Eq. 4 for each size class s by the integration of w during the entire renewal process comprised of n samples

$$w_{s,i} = \frac{1}{2}\left(M_{P,s,i-1}X_{s,i-1} + M_{P,s,i}X_{s,i}\right) \tag{2}$$

$$E_{s,t} = \frac{w_{s,t}}{W_s} \tag{3}$$

$$W_s = \sum_{i=1}^{n} w_{s,i}\cdot(t_i - t_{i-1}) \tag{4}$$

Note that E is not in strict terms the product residence time distribution, RTD. It is the exit age distribution, AD, of the material borne at the wall after atomization restarts. It includes the residence time that it takes for a granule at the wall to be re-entrained, plus its air-borne residence time to the exit. To facilitate the comparisons across the different size ranges, E are normalized in Eq. 3 by the mass re-entrained within each fraction W_s. The set of functions provided in Figures 12 and 13 can be interpreted directly as the probability of the material that is re-entrained within a given size range s to exit at a given time t. Logarithmic plots allow a better visualization when a distribution presents a very long tail. For this reason, a density function, E_{lg}, based on a logarithmic time is also calculated in Eq. 5

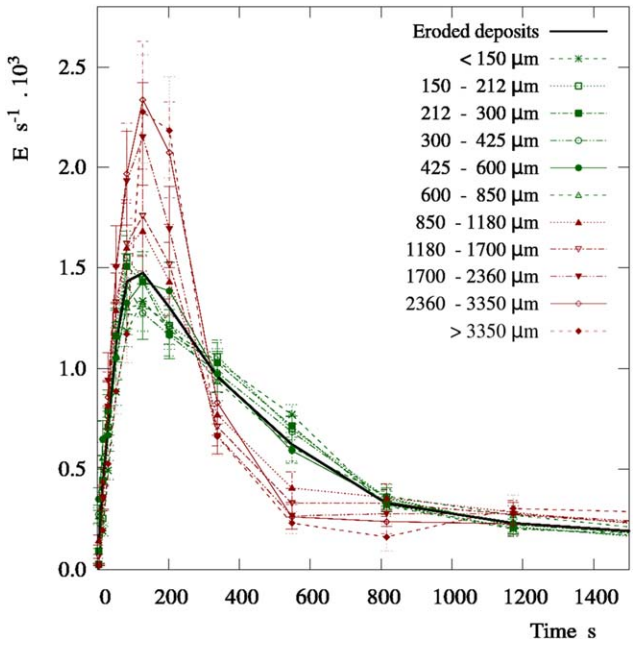

Figure 12. Detail of *E*.

Comparison between the mass averaged value and the functions for all size classes. [Color figure can be viewed in the online issue, which is available at wileyonlinelibrary.com.]

$$1 = \int_0^{\infty} E_s(t) \cdot dt = \int_0^{\infty} E_{\lg,\ s}(t) \cdot d(\lg\ t) \tag{5}$$

The mean or average residence time $\bar{t}$ is given as the first moment of E is provided in Eq. 6

$$\bar{t}_s = \int_0^{\infty} t \cdot E_s(t) dt \tag{6}$$

Table 2 summarizes the statistics of E. A characteristic mode occurs between the samples at 157.5 and 247.5 s, while t_{84} ranges from 1350 to 1720 s depending on the size of aggregates. The median age t_{50} and the mean $\bar{t}$ range between 310–510 s and 710–870 s, respectively. These values are, in average, from 10-100 times higher than the residence time expected from the trajectories of the air-borne particles in similar units,[22,28] <30 s or more recent numerical simulations in the same dryer[29,30] which report much lower values for the largest particles. The large time that the particles spend at the wall may explain why current models struggle to explain how drying occurs in such short air-borne residence times.

As time progresses the relative error in E becomes higher due to the smaller concentrations of dye. The tail of the distribution prolongs for a long time and at the final part, a large section is defined by fewer samples. This lead to a higher uncertainty in w and the integration in Eq. 4 explains why the confidence intervals in t_{50} and t_{84} are larger. This is particularly relevant for the largest granules which show a secondary peak at larger times.

Time scales in the re-entrainment mechanics

The same correlation between the aggregate size and the dye distribution appears in the analysis of the AD. The AD of the whole re-entrained material is compared with those of each size fraction in Figure 12. Two distinct groups can be distinguished: one is related to smaller fractions than the average product, another to large granules >850 μm. These are split in Figures 13ab and 13cd.

The smaller fractions result from the re-entrainment of pure particles and present a wide span in Figure 13a. In particular, the fractions <300 μm present a secondary peak between 300 and 600 μm and a prolonged exponential decay. As expected, fractions close to the mean sizes follow closely the average AD. The distributions obtained in the large fractions are shown in Figure 13c. As the size rises >850 μm, the history of the granules starts to include the aggregation of air and wall-borne material and the function changes, deviating from an exponential decay. The set of functions obtained is now clearly different from the average, and progressively narrows around the mode with increasing particle size. In addition, a secondary peak appears in all the fractions between 1100 and 1700 s. The logarithmic plots in Figures 13b and d illustrate how it gains relevance in the largest granules. The span of this peak cannot be estimated accurately but it is worth observing that this feature explains why the average statistics of large fractions are similar in Table 2 to the average and small sizes. Yet, Figure 13 shows that the AD functions have a clearly different nature.

The decrease of E given in Figure 13a could be approximated to a series of exponential decays characteristic of continuous stirred tank reactors, CSTR. However, these sizes exit as dyed pure particles, which discard the assumption of the release from a well-mixed layer. The slow decrease here rather than mixing indicates the kinetics of the renewal. Notice that the probability of the particle impacts to re-entrain dyed clusters from the outer layers decreases with t, as they renew and the surface of the wall exposing dyed sections decreases. In Figure 13c, ADs tend to be closer to an ideal plug flow reactor, PFR, with axial dispersion, than they are to a CSTR. This indicates that again, despite being mixtures, large granules do not come from a well-mixed structure that renews gradually. This would result in the exponential decay of E, where the mixtures would be released gradually. The re-entrainment, however, seems to occur at a faster time scale that produces mixtures from the first moment, which then exit with a narrow age range.

The distributions shown in Figure 13 fit well to a system of ideal reactors. In particular, the inflexion point in the

Table 2. A Summary of the Statistics of the Exit Age Distribution *E* of the Re-Entrained Material

Class x_{Max}	t_{16}	t_{50}	t_{84}	$\bar{t}$	$X_{s,o}$
μm	× 10^2 s	× 10^2 s	× 10^2 s	× 10^2 s	× 10^2
< 150	1.6 ± 0.1	5.0 ± 0.3	15.6 ± 2.1	7.9 ± 0.4	30 ± 2
to 212	1.4 ± 0.1	4.5 ± 0.5	13.5 ± 2.7	7.4 ± 0.6	29 ± 2
to 300	1.4 ± 0.1	4.6 ± 0.6	14.6 ± 3.3	7.6 ± 0.7	23 ± 2
to 425	1.5 ± 0.1	4.9 ± 0.7	15.0 ± 3.4	7.8 ± 0.8	19 ± 1
to 600	1.4 ± 0.1	4.7 ± 0.7	15.1 ± 3.2	7.8 ± 0.7	18 ± 1
to 850	1.5 ± 0.1	5.1 ± 0.8	15.2 ± 3.0	8.1 ± 0.8	21 ± 2
to 1180	1.3 ± 0.1	5.0 ± 1.4	16.0 ± 3.4	8.2 ± 1.0	33 ± 3
to 1700	1.3 ± 0.1	5.1 ± 1.6	17.2 ± 3.4	8.4 ± 0.9	46 ± 3
to 2360	1.2 ± 0.1	4.1 ± 1.5	16.2 ± 3.1	8.1 ± 0.9	34 ± 3
to 3350	1.1 ± 0.1	3.1 ± 0.7	14.5 ± 3.5	7.1 ± 1.0	31 ± 3
>3350	1.4 ± 0.1	4.0 ± 1.6	16.8 ± 2.0	8.7 ± 0.9	27 ± 2
Total	**1.4 ± 0.1**	**4.7 ± 0.3**	**15.1 ± 1.3**	**7.8 ± 0.3**	**20 ± 1**

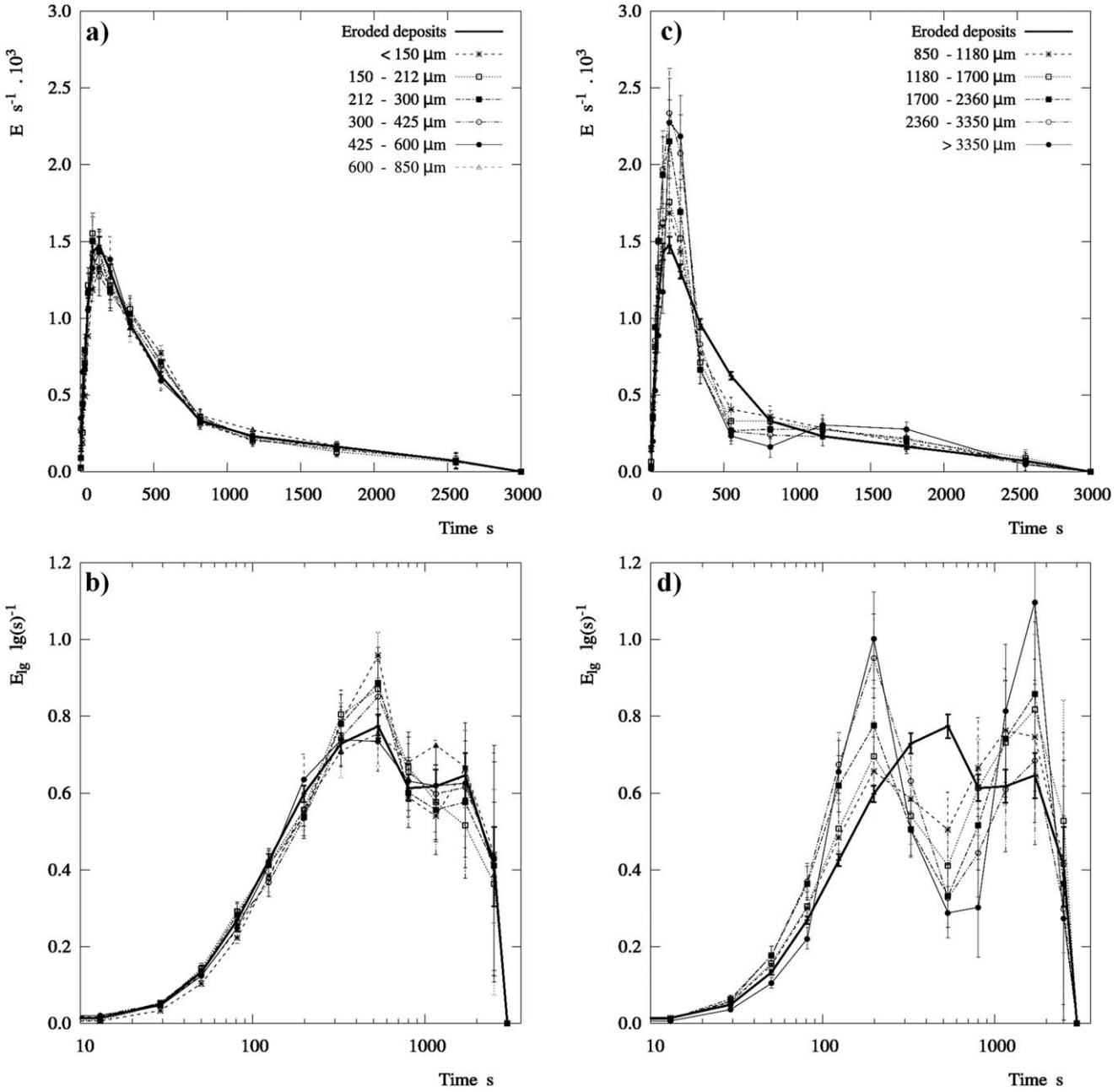

Figure 13. Age distribution of the re-entrained material, E and E_{lg}.

A comparison between the mass averaged value and the functions for the small and average size classes (a and b) and the large size classes (c and d).

average profile fits well with a system with two CSTRs in parallel.[27] In each branch, one CSTR followed by one PFR can represent the time particles spend in the deposits and the flow from the re-entrainment to the exit. A large or a small CSTR in each branch can be used to approximate respectively the long or short time scales observed in the re-entrainment. However, it is important to note the limitations of such approaches. The values of E reported here are in effect an average over the entire deposits' surface, which is itself very heterogeneous, see Figures 2 and 6. Deposits are not a well-mixed structures, but layers that grow in thickness and then break up. This very likely happens at different time scales in different sections because of the changes in the properties of the deposits (e.g. water content) and the stresses they are subject to (e.g. drag or particle impacts). This type of spatial effects cannot be described accurately by an ideal CSTR approximation. The secondary peak in Figure 13d and the corresponding shoulder in all smaller classes in Figure 13b provide a good example. It cannot be explained by a gradual renewal of outer layers because it owes to a sharp change in the re-entrainment rate: a significant part of the deposits exit at a time scale one order of magnitude higher than the mode, and twice higher than the mean. Such a sudden change could be linked to areas of the wall dominated by shedding, or detachment of large sections. This intermittent phenomenon is a common observation in dryers[24] and can release a considerable mass (see the final note in the experimental procedure).

To sum up, Figure 13 demonstrates that re-entrainment occurs at various time scales, which are correlated with the

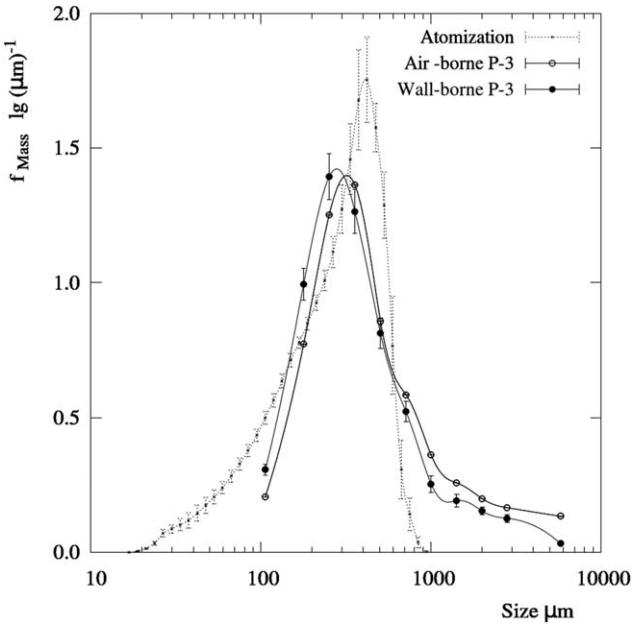

Figure 14. Size probability density functions for the droplets and the air and wall-borne material.

final granule size. In combination with the morphology analysis, it appears that fast and slow time scales are associated respectively to re-entrainment of granules with and without the aggregation with air-borne material.

Exit size of air and wall-borne material

The size distributions of air-borne and wall-borne material are compared with the initial droplet size in Figure 14. The eroded material has a higher proportion of smaller fragments but both present similar tails and a size distribution that shows a clear growth from the atomization to the exit. Bearing in mind that there are no particular differences in the morphology of pure particles, air-borne (white) or wall-borne (dyed), there is no evidence to suggest that they have been formed in a different way. The question remains on whether the growth occurred (1) before they were deposited, that is, coalescence, (2) upon the deposition itself, (3) during a long time in wall-borne state, or (4) after re-entrainment. Nonetheless, note that the population of pure white particles may have also interacted with the deposits but at faster time scales than the measurement, and thus the level of interaction with the wall can be higher than the reported by *X*. The same origin can be thought for the mixtures, with the obvious exception of having aggregated before deposition. The likelihood of the different hypothesis will be analyzed in the next section.

A Wall Dynamics Framework for Swirl Assisted Dryers

This section discusses the most likely dynamic of deposition and re-entrainment within countercurrent swirl dryers, and highlight specific areas for research. An outline is provided in Figure 15, which depicts the aging process and different contact mechanics by which the air-borne product may interact with the multilayer structure. It considers the re-entrainment associated to the action of aerodynamic forces, gravity, and the impact of wet droplets and dry particles, which lead to dry and wet mechanisms of erosion, and cause the detachment and breakage of large clusters.

Deposition and contact mechanics

Particle-droplet impacts[32] or droplet coalescence are largely studied at a small scale,[33,34] particularly in sprays.[35,36] Kinetic descriptions are also available in macroscale, for instance in the use of viscous and deformation Stokes numbers in wet granulation, which applies to granules with an elastic core and an outer binder layer.[37,38] The contacts described in Figure 15 for a spray drying context involve higher viscous forces and different structures. Here, particles/droplets have a wide range of viscosities and show a hard outer crust and a soft core.[39] Some authors approximate these collisions as the interpenetration of viscous spheres of a constant shape[40] but only recently detailed experiments have been made available[41] to provide data for advanced numerical models.[42] The impacts to a fix substrate can be thought in very similar terms, but need to recognize the role of the microstructure, that is, how the cohesive forces drive the behavior of the wall-borne clusters. The time scale and the contact area developed in an impact depend on the drying state of deposits and the impacting droplet, and the impact inertia. Deposition occurs only if the adhesive force generated is higher than the aerodynamic disruptive stresses of a similar time scale, plus those from an inertial source: (1) the shear stress caused by gravity and the centrifugal inertia and (2) the elastic recovery which causes a normal detaching force.

Impacts between sufficiently dry partners, denoted by stage [11] in Figure 15, result in rebound in stage [14]. The bonds between wall-borne clusters, however, need sustaining the stresses derived from the impact. If they are large enough, they may cause the breakage of the microstructure and re-entrainment in [11, 12, 13], or in [11, 12, 5, 6, 7] denoted as dry erosion or shedding, described later. Impacts develop a larger contact area when the droplets are deformable in stage [1]. Two possibilities may be considered. One, deposition at low inertias in [2], where both adhesive (droplet-cluster) and cohesive forces (between clusters) sustain the impact stresses. Another, at high inertias in [8]: the larger droplets impact the wall at high velocity, which generates a larger contact area and a higher shear stress. Capture occurs when the shear stress breaks the bridges between neighboring clusters but the adhesive forces between the droplet and the cluster can sustain it, see stages [1, 8, 9] or [1, 8, 5, 6, 7] in Figure 15, denoted wet erosion or shedding and described later.

Other factors, such as wall roughness and particle shape play an important role in the contact mechanics. The balance of forces established depends greatly on the disposition of the roughness[9] and the sole action of the heterogeneities owed to the deposits has an important effect in particle flow and residence time.[43,44] Consider that in this case, the surface features of the clusters at the wall are very large, comparable to the cavities of impacting particles, if not the particles themselves, see Figures 9 and 16, and Supporting Information. In addition, elutriated fines contain many ligaments produced during atomization, which appear as coiled structures in the product, see Figure 16. In this context, particles can get trapped at the wall by simply locking or rotating in the cavities of the outer layers. This would increase significantly the residence time and may explain the difference between the mode residence time of the large re-entrained granules in

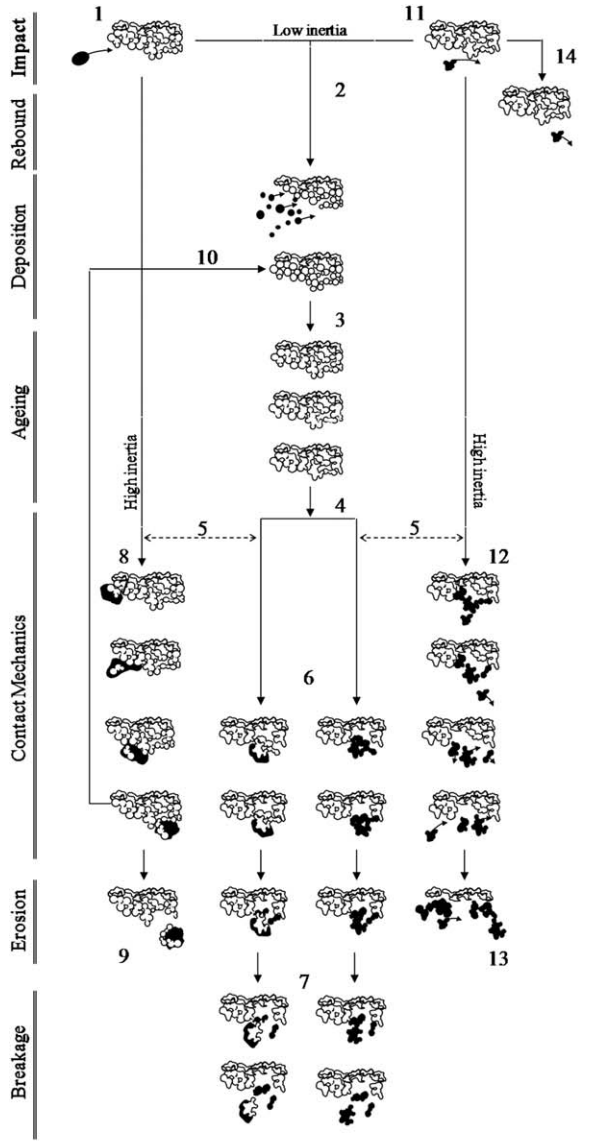

Figure 15. Wall dynamics in countercurrent spray drying.

Contact mechanics leading to erosion, aggregation and the breakage of clusters at a multilayer structure.

Figure 13c (between 157.5 and 247.5 s) and the air-borne residence time expected from models.

Aging

The particle-particle forces at the deposits evolve as time progresses in stage [3]. New bridges are formed by deposition in [2] and [10] and the existing ones solidify, becoming more porous and brittle.[45–47] In addition, as the layer grows, the clusters start containing higher numbers of primary particles but are sustained by a lower specific contact area, which facilitates their removal due to gravity.

The evolution of the contacts (see Figure 16) responds to the rates of different transport phenomena, some of which are described for the erosion of ash deposits.[11] On one hand, external heat and mass transfer rates dry the structure, increase its porosity, and accelerate the crystallization of salts, and on the other hand, large differences in the water content facilitate the migration of species. These are long time scale processes that occur in parallel with the momentum transfer driven by impacts, the action of the Laplace pressure and gravity. Their combination ultimately determines the sintering rate. It is important to advance in the evaluation of the relative time scales of these phenomena because properties such as viscosity or water diffusion coefficients vary across several orders of magnitude as the material dries at the wall. Ultimately, the time it takes for the viscous-like material deposited to turn into a deformable solid will constrain the rate at which bridges such as those shown in Figure 16 can thin or sinter.

Origin of the disruptive stresses

The multilayer at the walls breaks when it cannot sustain the stresses caused by the inertia of the impacts, gravity and the drag and lift forces caused by the air flow. However, it is interesting to note that when the tower is empty, re-entrainment stops (see the final note in the experimental procedure). Thus the particle impacts must be necessary to trigger it. This can be explained by (1) outer layers growing sufficiently so that gravity cause the detachment in stages [2, 3, 4, 5, 6, 7] in Figure 15, or (2) breakage due to the impact of dry particles in [11, 12, 13] or wet droplets in [1, 8, 9]. In each case, re-entrainment occurs at very different time scales: (1) a long one occurs after deposition, aging, and shedding so that the size of the re-entrained cluster is related to the microstructure of the multilayer, and (2) a short one occurs as a result of impacts, and thus the size of the re-entrained cluster is also related to the properties of the particles or droplets responsible.

In stage [6], gravity and aerodynamic forces alone may suffice to induce the removal of clusters when they grow. Now, this implies the aggregation between new droplets and the wall-borne clusters, and as such, we should expect the product to be comprised in general of mixtures. Indeed, this occurs for the large granules but it does not for most of the product. The next section discusses several re-entrainment mechanisms that can explain this behavior.

Mechanisms of re-entrainment

The material bounded at the multilayer exits the unit in two different populations: (1) a set of granules is re-entrained directly with no aggregation and at a long time scale, and (2) another set, >850 μm, is comprised of aggregates of wall-borne clusters and air-borne droplets and exits at much shorter time scale. Both show intermittencies.

Dry Mechanisms of Erosion. Multiple impacts of dry particles with sufficient inertia to break bonds within the structure of the deposits cause the direct re-entrainment of aggregates, see stages [11, 12, 13] in Figure 15. In combination with gravity, it may be also responsible of triggering the detachment of larger pieces and their subsequent breakage in [11, 12, 5, 6, 7]. This type of contact is associated with both, drier particles and drier sections of the

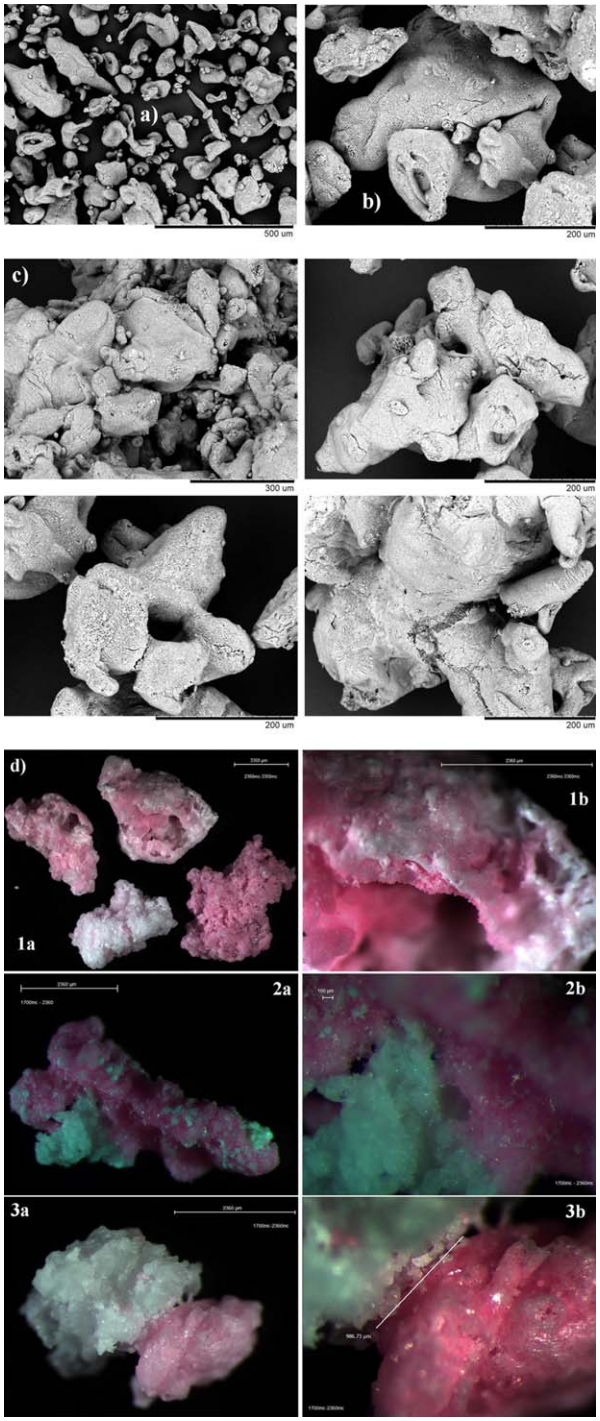

Figure 16. (a) Ligaments in the elutriated fines, (b) coiled structures in the product, (c) solid bridges, (d) contact of air- and wall-borne material: layering (1b) solid bridges (2, 3).

Micrograph (1) shows the size fraction 2360 μm<x_p<3350 μm; (2, 3) 1700 μm<x_p<2360 μm. Scale bars: 3350 μm in (1a); 2360 μm in (1b, 2a, 3a); 100 μm in (2b) and 986 μm in (3b). [Color figure can be viewed in the online issue, which is available at wileyonlinelibrary.com.]

multilayer (above and below the projection of the nozzle in Figure 2). In this case, re-entrainment occurs as a single event and for this reason, one may associate the long decay in E in Figure 13a to the time that particles remain fixed at the wall rather than to the time of flight between the wall and the exit.

The lack of mixtures is noticeable. Pure re-entrained particles do not appear to have sintered with the newly deposited material, which has two possible explanations. One is that drying fixes their size after deposition and suppresses sintering. This suggests that growth occurred before the time at the wall, for example, during coalescence, or at the deposition impact itself. Another explanation comes from the production of pure particles by breakage in stage [7]. In this case, the largest granules are more likely to survive containing the mixed regions, leaving smaller particles pure.

Wet Mechanisms of Erosion. A part of the re-entrained deposits exits after having aggregated with air-borne material and presents a clearly different residence time. The mixed granules must be produced by (1) aggregation on the deposition of new droplets, (2) sintering in a wall-borne state, or (3) contacts after the erosion. The latter implies coating after numerous impacts with small droplets or the capture by large ones. Both are very unlikely given the low concentrations away from the wall.[24] In regards to sintering, it may be responsible of the formation of solid bridges, but it does not generate the mixtures because they exit not only at large times but from the first moment.

The most likely origin for the mixtures is direct growth on the impact of wet droplets in [8] in Figure 15. These present the largest inertia and are common in the area of the spray projection. Here, droplets >200 μm still have high water contents and momentum when they impact the wall, which occurs with a significant tangential component. On colliding, they deform, lose energy due to viscous dissipation and capture aggregates, either in close proximity to the wall or already bounded at the structure. Stages [1, 8, 9] in Figure 15 describe a rolling mechanism whereby wall-borne clusters act as initial rigid nuclei that becomes encapsulated. This appears as a likely contact mechanics in agreement with the morphology observed in Figure 11 and similar "Rock'n Roll" mechanisms proposed for resuspension of single particles.[5,7,48] Newly formed encapsulates may deposit in [10], roll or saltate along the surface, or become detached in [9]. If rolling or saltation occurs, the granule may keep picking up clusters in a snowball effect. Its ability to grow would quickly decrease as the surface dries and the inertia dissipates.

As opposed to dry erosion, re-entrainment now is comprised of multitude events occurring at fast time scales. For that reason, the first mode in Figure 13c can be thought to be related not to the time in a wall-borne state, but rather to the air-borne history which is obviously affected by numerous contacts with the wall. The mode residence time reported may be related to the saltation of granules documented before in the same type of dryers.[24] It may correspond to the time it takes for wet large granules, initially formed close to the nozzle projection, to saltate down the surface of the chamber, growing as they come in contact with the wet areas of deposits.

Shedding and Breakage. Deposits in Figure 6 show large variations in thickness, and identifiable groups of clusters at the surface. This is the result of a shadow effect (i.e. the heterogeneity of the outer layer makes particles to pile onto the same area rather than distribute homogenously). This is

emphasized in this case by nonspherical shapes and the low impact angles to the wall.

As the clusters grow, they become destabilized and can detach in stage [6]. As described before, shedding may be triggered directly by the growth of the layer or by the impact of particles/droplets at high inertia in [5]. Once large pieces are detached, they are not likely to sustain the stresses in an air-borne state and break down into smaller fragments in [7] which contain both, pure particles or mixtures depending on whether the initial impact involved wet droplets or dry particles in [1, 8, 5, 6, 7] or [11, 12, 5, 6, 7] or both if the detachment was purely triggered by gravity in [2, 3, 4, 5, 6, 7]. The presence of these intermittent events may explain the largest time scale features observed in the AD.

Conclusions

This work demonstrates that the wall dynamics can have a major impact in swirl countercurrent spray dryers:

a. *Rate*: In the context of detergent manufacture, deposition and re-entrainment are found to be in equilibrium for the most relevant section in the dryer. The re-entrainment rate comprises >12–20%. in mass of the full production, becoming higher for both smaller size fractions and particularly aggregates >850 μm in diameter.

b. *Time scale*: The mechanics of re-entrainment varies for aggregates of different size. Small and average size particles are directly re-entrained with no aggregation with air-borne material. In contrast, aggregates >850 μm appear as mixtures of both and thus are almost entirely originated in cycle of deposition and re-entrainment. However, no differences are appreciated between the morphology of pure re-entrained particles and the rest. Bearing in mind that the re-entrainment rates given are under predictions, the level of interaction with the multilayer may be much higher. The time scale of this equilibrium has also an important effect in the residence time of the product, thus affecting its drying. The material undergoing the wall cycle has a residence time 10–100 times higher than the values expected from their air-borne trajectories. Such a large deviation represents a serious handicap in numerical models, which neglect the largest proportion of the time that the re-entrained product remain exposed to heat and mass transfer rates.

c. *Growth and Structure*: Different re-entrainment time scales have been identified as the responsible of producing resuspension of deposits either with or without the aggregation with air-borne material. These have been correlated respectively with the generation of most of the aggregates >850 μm and a fraction of the smaller and averaged sized particles. Accordingly, a series of mechanisms has been proposed to describe this process. They include the re-entrainment caused by the impact of dry particles, capture and aggregation caused by the impact of wet droplets, and their combination with gravity to cause the detachment of large clusters and their breakage.

In summary, this work proposes a residence time approach to the characterization of fouling, applicable to other systems subject to particulate deposits. It highlights the relevance of deposition, aging, and re-entrainment in swirl spray dryers. Their effect goes beyond prior considerations, dominating the drying kinetics, the particle growth, and the structure of a significant proportion of the product, at least under detergent manufacture. Numerical models based exclusively in the description of the fluid dynamics and particle processes during their flight in the dryer are not sufficient to describe the process. Addressing this limitation implies being able to describe the structure of the deposits and the mechanics governing its renewal. This could led to a better control of re-entrainment rate and the product properties, for instance adjusting operating conditions such as the swirl intensity, the flow kinetic energy or the slurry formulation.

Acknowledgments

VF was supported by an Engineering Doctorate Studentship sponsored by the Engineering and Physical Sciences Research Council (EPSRC) and Procter & Gamble in the Industrial Doctoral Centre in Formulation Engineering, School of Chemical Engineering, University of Birmingham. The authors thank Mr. Andrew Roberts, Mr. Dave Banks, and the tower operation crew at P&G in Newcastle upon Tyne for their commitment in the coordination and execution of the experiments.

Notation

A = absorbance
D = tower diameter, m
E = age probability density function, s^{-1}
H = distance from air inlets to vortex finder, m
M = total mass in the wall plate, kg
M_P = product mass rate from the tower belt, kg s^{-1}
M_E = mass rate of elutriated powder from the cyclones, kg s^{-1}
M_{PE} = powder mass rate exiting the dryer, kg s^{-1}
S = dilution factor, m^3 kg^{-1}
T = temperature, °C
W = dyed material exited in a given time and size range, kg
X = ratio of wall-borne material
d = diameter of the vortex finder, m
f = size frequency, $lg(\mu m)^{-1}$
r = mass rate, kg s^{-1}
t = time, s
w = exit rate of dyed material (wall-borne material), kg s^{-1}
x_p = particle diameter, μm
z = distance to the air inlets, m

Subscripts

IN = for the inlet air line
EX = for the exhaust (exit) air line
A = for the air
P = for the product exiting from the tower belt
S = for the slurry
d = deposition
e = erosion
cone = at a location in the conical section of the drier
final = at the average of the steady state period
lg = based in the logarithm of time t
max = upper side of an interval
n = time range
t = at time t, or in sample at time t
o = initial or at the initial sample
ref = for the reference obtained on P−2
s = size fraction
St = at the steady state

Literature Cited

1. Papavergos PG, Hedley AB. Particle deposition behaviour from turbulent flows. *Chem Eng Res Des*. 1984;62:275–295.
2. Ziskind G, Fichman M, Gutfinger C. Resuspension of particulates from surfaces to turbulent flows. *Review and analysis. J Aerosol Sci*. 1995;26:613–644.

3. Soldati A, Marchioli C. Physics and modeling of turbulent particle deposition and entrainment: review of a systematic study. *Int J Multiphase Flow*. 2009;35:827–839.
4. Henry C, Minier JP, Lefevre G. Towards a description of particulate fouling: from single particle deposition to clogging. *Adv Colloid Interface Sci*. 2012;185–186:34–76.
5. Reeks MW, Hall D. Kinetic models for particle resuspension in turbulent flows: theory and measurement. *Aerosol Sci*. 2001;32:1–31.
6. Reeks MW, Reed J, Hall D. The resuspension of small particles by a turbulent flow. *J Phys D*. 1988;21:574–589.
7. Zhang F, Reeks MW, Kissane M. Resuspension of small particles from multilayer deposits in turbulent boundary layers. In: *International Conference in Multiphase Flow*. Jeju, South Korea, 2013.
8. Zonta F, Marchioli C, Soldati A. Particle and droplet deposition in turbulent swirled pipe flow. *Int J Multiphase Flow*. 2013;56:172–183.
9. Guingo M, Minier JP. A new model for the simulation of particle resuspension by turbulent flows based on a stochastic description of wall roughness and adhesion forces. *Aerosol Sci*. 2008;39:957–973.
10. Marshall JS. Particle aggregation and capture by walls in a particulate aerosol channel flow. *J Aerosol Sci*. 2007;38:333–351.
11. Wang H., Harb JN. Modeling of ash deposition in large-scale combustion facilities burning pulverized coal. *Prog Energy Combust Sci*. 1997;23:267–282.
12. Zbogar A, Frandsen F, Jensen PA, Glarborg P. Shedding of ash deposits. *Prog Energy Combust Sci*. 2009;35:31–56.
13. Bashir MS, Jensen PA, Frandsen F, Wedel S, Johansen KD, Wadenbäck J, Pedersen ST. Ash transformation and deposit build-up during biomass suspension and grate firing: full-scale experimental studies. *Fuel Process Technol*. 2012;97:93–106.
14. Kota K, Langrish TAG. Fluxes and patterns of wall deposits for skim milk in a pilot-scale spray dryer. *Dry Technol*. 2006;24:993–1001.
15. Epstein N. Thinking about heat transfer fouling: a 5x5 matrix. *Heat Transfer Eng*. 1983;4:43–56.
16. Ozmen L, Langrish TAG. An experimental investigation of the wall deposition of milk powder in a pilot-scale spray dryer. *Dry Technol*. 2003;21:1235–1252.
17. Langrish TA, Zbiciński I. The effects of air inlet geometry and spray cone angle on the wall deposition rate in spray dryers. *Chem Eng Res Des*. 1994;72:420–430.
18. Hanus MJ, Langrish TAG. Re-entrainment of wall deposits from a laboratory-scale spray dryer. *Asia-Pac J Chem Eng*. 2007;2:90–107.
19. Kota K, Langrish TAG. Prediction of wall deposition behaviour in a pilot-scale spray dryer using deposition correlations for pipe flows. *J Zhejiang Univ Sci A*. 2007;8:301–312.
20. Hanus MJ, Langrish TAG. Resuspension of wall deposits in spray dryers. *J Zhejiang Univ Sci A*. 2007;8:1762–1774.
21. Woo MW, Daud WRW, Mujumdar AS, Tasirin SM, Talib MZM. Role of rheological characteristics in amorphous food particle-wall collisions in spray drying. *Powder Technol*. 2010;198:252–257.
22. Huntington DH. The influence of the spray drying process on product properties. *Dry Technol*. 2004;22:1261–1287.
23. Palzer S. Agglomeration of pharmaceutical, detergent, chemical and food powders. Similarities and differences of materials and processes. *Powder Technol*. 2011;206:2–17.
24. Hassall G. Wall build up in spray driers. EngD Thesis. Birmingham, UK: University of Birmingham, 2011.
25. Francia V, Martin L, Simmons MJH, Bayly AE. Deposition and wear of deposits in swirl spray driers: the equilibrium exchange rate and the wall-borne residence time. In Press. Procedia Engineering. *Proceedings of the 7th World Congress in Particle Technology*. Beijing, China, May 19–22, 2014.
26. Francia V, Martin L, Simmons MJH, Bayly AE. An experimental investigation of the swirling flow in a tall-form counter current spray dryer. *Exp Therm Fluid Sci*. In Press. DOI: 10.1016/j.expthermflusci.2015.03.004.
27. Levelspiel O. *Ingeniería de las reacciones químicas (Chemical Reaction Engineering)*, 3rd ed, Mexico, Limusa Wiley, 2004.
28. Harvie DJE, Langrish TAG, Fletcher DF. A computational fluid dynamics study of a tall-form spray dryer. *Trans IChemE*. 2002;80:163–175.
29. Ali M, Mahmud T, Heggs PJ, Ghadiri M, Francia V, Bayly AE, Djurdjevic D, Ahmadian H, Martin L. CFD modeling of a counter-current spray drying tower. In: *International Conference in Multiphase Flow*. Jeju, South Korea, 2013.
30. Ali M. Numerical modelling of a counter-current spray drying tower. PhD Thesis. Leeds, UK: University of Leeds, 2014.
31. Francia V. Spray drying of detergents in counter current towers: a study of turbulent swirling flows, fouling and agglomeration. EngD Thesis. Birmingham, UK: University of Birmingham, 2015.
32. Dubrovsky VV, Podvysotsky AM, Shraiber AA. Particle interaction in three-phase polydisperse flows. *Int J Multiphase Flow*. 1992;18:337–352.
33. Qian J, Law CK. Regimes of coalescence and separation in droplet collision. *J Fluid Mech*. 1997;331:59–80.
34. Liao Y, Lucas D. A literature review on mechanisms and models for the coalescence process of fluid particles. *Chem Eng Sci*. 2010;65:2851–2864.
35. Rüger M, Hohmann S, Sommerfeld M, Kohnen G. Euler/Lagrange calculations of turbulent sprays: the effect of droplet collisions and coalescence. *At Sprays*. 2000;10:47–81.
36. Post SL, Abraham J. Modeling the outcome of drop–drop collisions in diesel sprays. *Int J Multiphase Flow*. 2002;28:997–1019.
37. Liu LX, Iveson SM, Litster JD, Ennis BJ. Coalescence of deformable granules in wet granulation processes. *AIChE J*. 2000;46:529–539.
38. Iveson SM, Litster JD, Hapgood KP, Ennis BJ. Nucleation, growth and breakage phenomena in agitated wet granulation processes: a review. *Powder Technol*. 2001;117:3–39.
39. Handscomb CS, Kraft M, Bayly AE. A new model for the drying of droplets containing suspended solids. *Chem Eng Sci*. 2009;64:628–637.
40. Hoeven MJ. Particle-droplet collisions in spray drying. PhD Thesis. Queensland, Australia: School of Engineering, University of Queensland, 2008.
41. Kuschel M, Sommerfeld M. Investigation of droplet collisions for solutions with different solids content. *Exp Fluids*. 2013;54:1440.
42. Focke C, Kuschel M, Sommerfeld M, Bothe D. Collision between high and low viscosity droplets: direct numerical simulations and experiments. *Int J Multiphase Flow*. 2013;56:81–92.
43. Sommerfeld M. Modeling of particle-wall collisions in confined gas-particle flows. *Int J Multiphase Flow*. 1992;18;905–926.
44. Sommerfeld M, Huber N. Experimental analysis and modeling of particle-wall collisions. *Int J Multiphase Flow*. 1999;25:1457–1489.
45. Tardos GI, Gupta R. Forces generated in solidifying liquid bridges between two small particles. *Powder Technol*. 1996;87:175–180.
46. Farber L, Tardos GI, Michaels JN. Evolution and structure of drying material bridges of pharmaceutical excipients: studies on a microscope slide. *Chem Eng Sci*. 2003;58:4515–4525.
47. Bikaa D, Tardos GI, Panmaia S, Farbera L, Michaelsa J. Strength and morphology of solid bridges in dry granules of pharmaceutical powders. *Powder Technol*. 2005;150:104–116.
48. Vatistas NT. Effect of adhesion time on particle deposition: re-entrainment and rolling. *Ind Eng Chem Res*. 1992;31:1554–1559.

Manuscript received Oct. 16, 2014, and revision received Jan. 13, 2015.